Supporting information

Polydopamine-Wrapped, Silicon Nanoparticle-Impregnated Macroporous CNT Particles: Rational Design of High-Performance Lithium-Ion Battery Anodes

Experimental Section

Fabrication of PD / Si NPs / mCNTPs. Fabrication Polystyrene latex particles were synthesized by emulsifier-free polymerization. The CNT (JEIO) used was a 20 nm outer diameter multi-walled CNT and was dispersed in water using a surfactant (1wt%, Pluronic F-127, Sigma Aldrich). The Si nanoparticles (CNVISION) that were used possessed an average diameter of 80 nm. A mixture solution of polymer particles, CNTs, and Si NPs was prepared, and the total concentration was about 3 wt%. Spray drying was carried out at a rate of 12 ml min^{-1} at 140 °C, and then heat-treated at 500 °C for 2 hrs. The coating of PD was achieved by polymerization of dopamine (Aldrich) in the presence of the Si NPs / mCNTPs in 100 mL Tris-buffer (10 mM, pH 8.5). The synthesis proceeded at room temperature with stirring for 12 hrs. A mixture of the active material (70 wt%), a carbon-based conductive agent (DB-100, 15 wt%), and polyacrylic acid (PAA) binder (15 wt%) was prepared. The anode was prepared by coating this mixture onto a copper foil current collector.

Lithium ion battery assembly and characterization.

The battery performances were tested using a Maccor 4300 test system. CR2032 coin-type cells were assembled using Li metal foil as the counter electrode and a polypropylene membrane. The mass loading of the active materials for all samples was 1.55 mg cm-2. The gravimetric capacities that were determined are based on the mass of pure active materials excluding the conducting agents and binder. The liquid electrolyte was prepared by dissolving 1 M LiPF$_6$ in a mixture of ethylene carbonate (EC)/ethyl methyl carbonate (EMC)/dimethyl carbonate (DMC) (EC:EMC:DMC = 1:1:1). The electrochemical impedance

analysis was conducted by electrochemical impedance spectroscopy (EIS) using an impedance analyzer (Versastat, AMETEK). The frequency range was 1 MHz to 0.1 Hz, and the voltage amplitude was 10 mV.

Characterization.

A field-emission scanning electron microscope (Carl Zeiss) and transmission electron microscopy (JEOL) were used for SEM and TEM measurement, respectively. Raman spectra were recorded using a Horiba Jobin Yvon LabRam HR. X-ray diffraction patterns were obtained using a Davinci D8 Advance diffractometer. Thermogravimetric analysis (TGA) was conducted by TGA Q50 (TA instrument). BET pore characterization was achieved by ASAP 2020 (Micrometrics Inc.). The pore sizes and pore volumes were measured from pore size distribution curves determined from the Barrett–Joyner–Halenda (BJH) method.
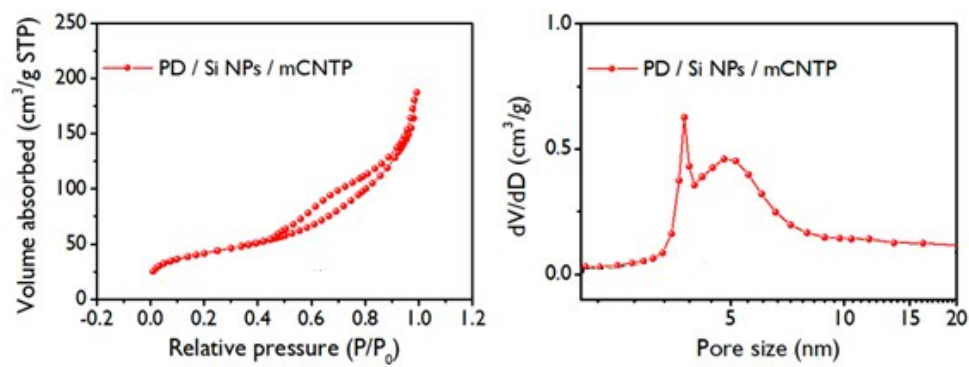
Fig. S1 Nitrogen adsorption/desorption isotherms and pore size distribution of the PD / Si NPs / mCNTPs.
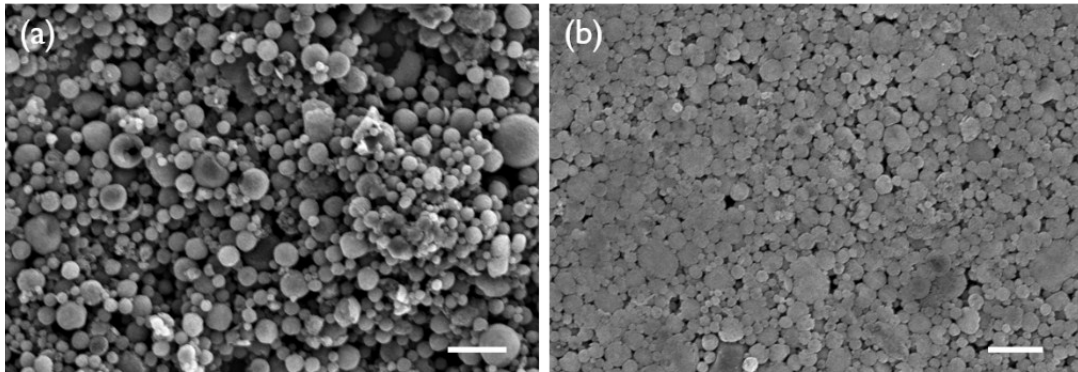
Fig. S2 SEM images of the PD/Si NPs/CNTP anodes (a) before and (b) after pressing.(Scale bar: 20 μm) It was confirmed that a spherical particle shape was maintained without fracture following pressing.
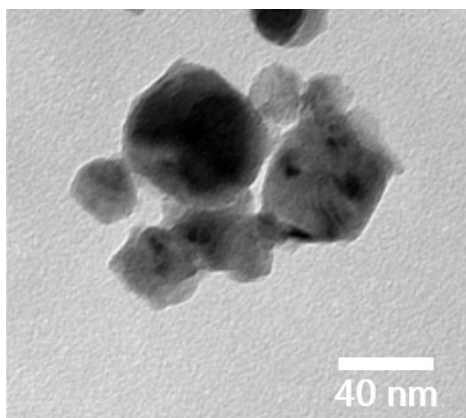
Fig. S3 TEM image of Si NPs
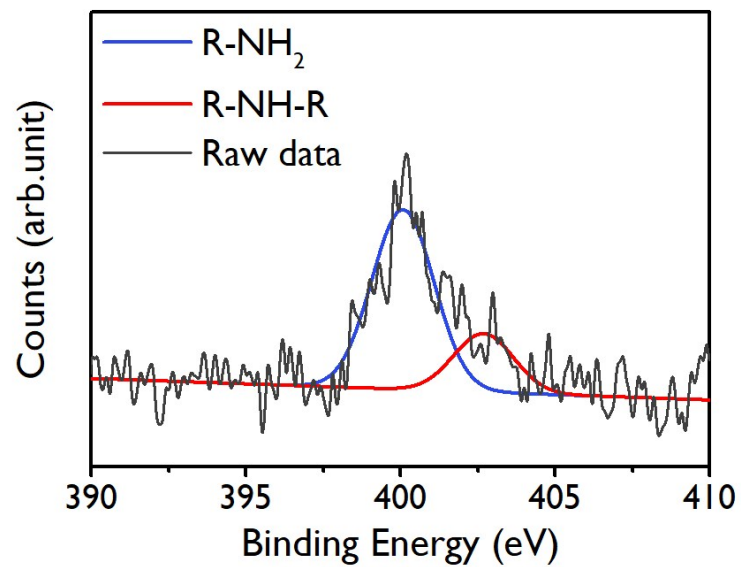
Fig. S4 The N 1 s XPS spectrum (gray line) of the PD/Si NPs/mCNTPs. The deconvoluted peaks of R-NH$_2$ and R-NH-R (colored lines) are indicated in each spectrum.
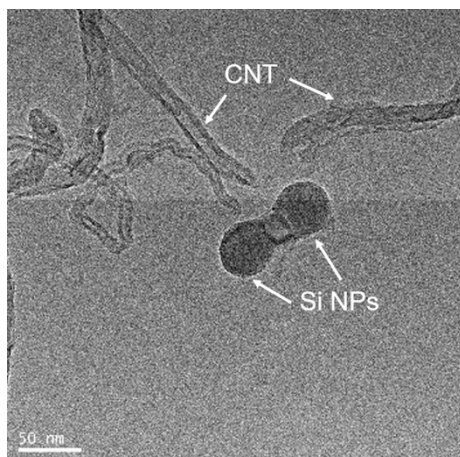
Fig. S5 TEM image of CNT/Si nanoparticles after ball-milling process. For samples without PD, in the same sample preparation, the Si NPs are separated from the CNTs; the adhesion between the Si NPs and CNTs is improved by the PD coating.
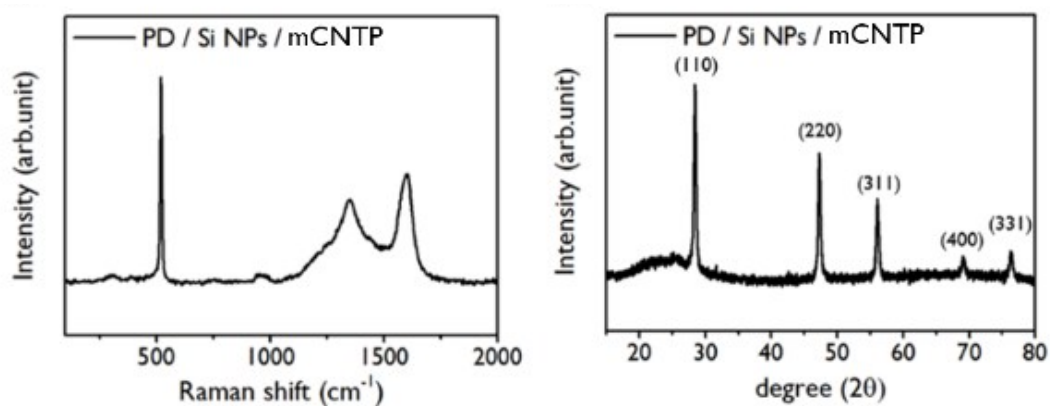
Fig. S6 (c) Raman and (d) XRD spectra of PD/Si NPs/mCNTPs. The Raman spectrum contained a strong peak at 517 cm^{-1}, which indicates a crystalline Si phase. The Raman spectrum also contained broad peaks at 1350 and 1595 cm^{-1}, which are the well-known defective (D) and graphitic (G) peaks of carbon.[1] The XRD pattern also displays the peaks for crystalline Si and the peak for CNT at 26°[2]
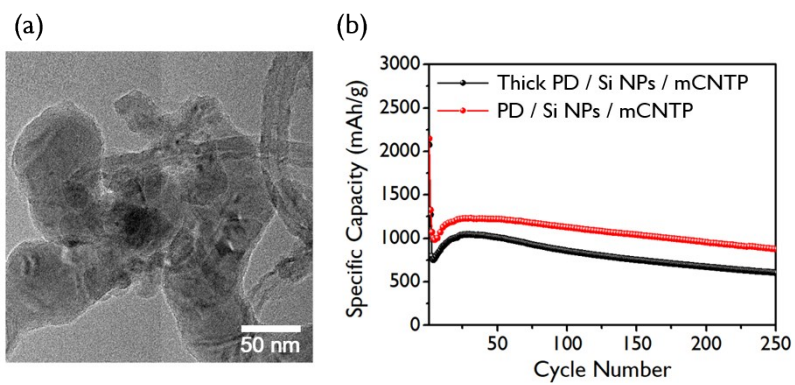
Fig. S7 (a) TEM image of Si NPs coated with thick PD. (b) Cycle performance of current electrode and thick PD wrapping electrode.
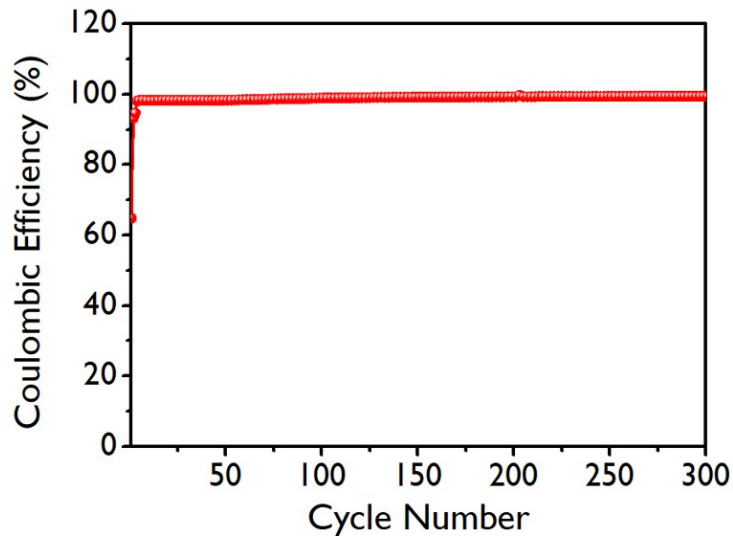
Fig. S8 Coulombic efficiency of the PD/Si NPs/mCNTPs anode cell. The initial coulomb efficiency is as low as 65%. Many Si-based anode LIBs have often shown similar low efficiencies.[3-5] Generally, the consumption of Li and the formation of the SEI layer by contact with the electrolyte deteriorate the coulombic efficiency. Most of the Si / C electrodes utilize high surface area nano Si and also have a porous structure for efficient volume penetration of electrolyte and relaxation of the volume expansion of silicon, resulting in low initial coulombic efficiency due to easy contact with the electrolyte.[6, 7]
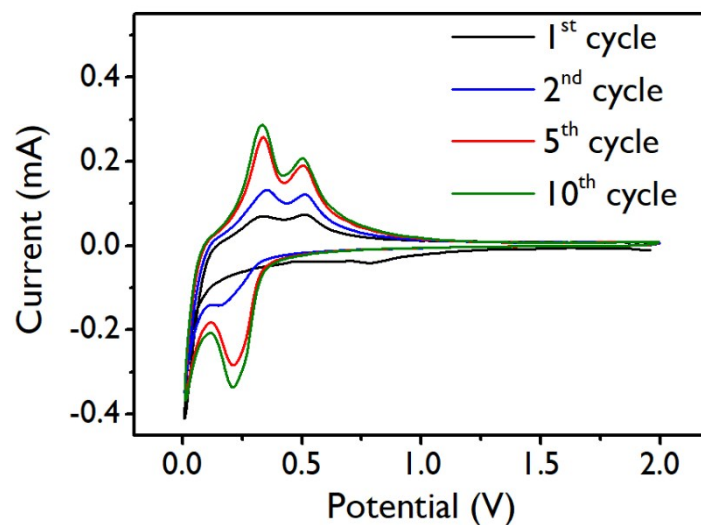
Fig. S9 Cyclic voltammetry of PD/Si NPs/mCNTP between 2 and 0.01 V with a scan rate of 0.05 mV s^{-1}. The reduction peak at 0.7 - 0.8 V in the first cycle disappears in subsequent cycles, indicating the formation of an irreversible SEI layer in the initial cycle. The disappearance of the peak in subsequent cycles implies the formation of a stable SEI layer, which is stabilized by PD wrapping.
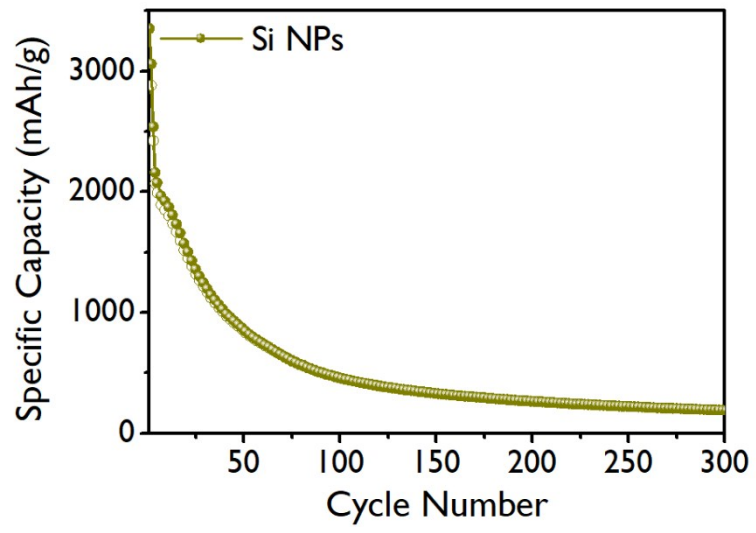
Fig. S10 Cycle performance of Si NPs anode cell.
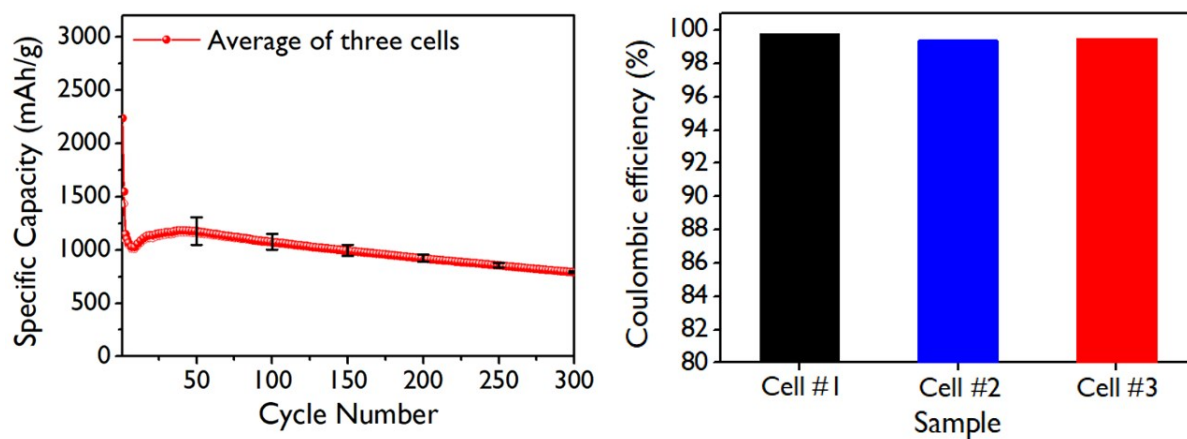
Fig. S11 (left) Average cycle performance and error bar of three PD/Si NPs/mCNTPs anode cells at 2 A/g for 300 cycles after an initial cycle activation at 100 mA/g. (right) Coulombic efficiency of three PD/Si NPs/mCNTPs anode cells at 2 A/g after 300 cycles.
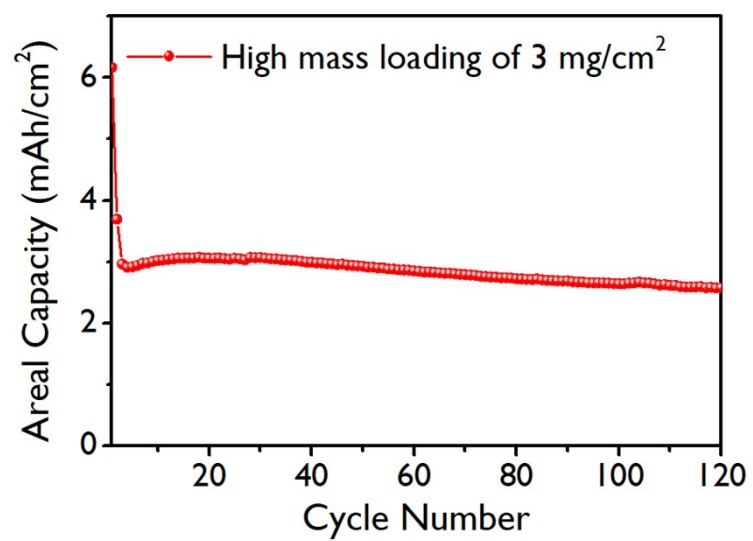
Fig. S12 Cycle performance of PD / Si NPs / mCNTP anodes with high areal mass loading of 3 mg/cm² (active material) at a current density of 0.25 mA/cm² after an initial two-cycle activation at 0.05 mA/g.

Table S1. Comparison of the specific capacity and cycle stability of Si-C composite electrode

in the literature

Materials	Specific capacity (Cycle No.)	Capacity retention (%)	Mass loading (mg cm^{-2})	Reference
Si@C hollow core-shell	618 m Ah g^{-1} (20 cycle)	75.9% (20 cycle)	-	8
Si@C yolk-shell	-	85% (100 cycle)	1 mg cm^{-2}	9
Si in porous carbon black cage	1300 m Ah g^{-1} (50 cycle)	84% (50 cycle)	0.6 mg cm^{-2}	10
C coated Si NPs cluster	557 m Ah g^{-1} (200 cycle)	44% (200 cycle)	1 mg cm^{-2}	11
Si in between the C core and C-shell	904 m Ah g^{-1} (100 cycle)	77.5% (100 cycle)	-	12
Si-N porous Carbon	1103 m Ah g^{-1} (100 cycle)	72% (100 cycle)	1 mg cm^{-2}	13
Si@AlF$_3$@C	1001 m Ah g^{-1} (125 cycle)	75.8% (125 cycle)	-	14
Si NPs/CNT/C fiber	1000 m Ah g^{-1} (100 cycle)	74.1% (100 cycle)	-	15
Hollow nanospheres / loosely packed Si/SiOx NP	940 m Ah g^{-1} (200 cycle)	92% (200 cycle)	-	16
hierarchical core-shell Si/C	903 m Ah g^{-1} (100 cycle)	89%	-	17

fiber		(100 cycle)		
Our work	1138/1128/956/795 m Ah g^{-1} (50/100/200/300cyle)	81% (300 cycle)	1.5 mg cm^{-2}	-

Table S2. Comparison of the capacity retention of Si-amorphous C composite electrode in the literature

Materials	Capacity retention (folds, %)	Reference
Nanocrystalline silicon@C	20-folds, 20%	[18]
Carbon coated Si nanorod	10-folds, 40%	[19]
Hollow Carbon/silicon/alumina sphere	8-folds, 46.4%	[20]
Yolk-shell Si@C	10-folds, 52.9%	[21]
Void-Involved Silicon/Carbon	6-folds, 43.6%	[22]
Corn-like mesoporous Si/N-Carbon layer	4-folds, 50%	[23]
Raspberry-like nanostructured silicon	8-folds, 41.7%	[24]
Our work	10-folds, 57%	

Table S3. Comparison of the areal capacity and cycle stability of Si based lithium ion battery electrode in the literature

Materials	Areal capacity (Cycle No.)	Capacity retention (%)	Current density (mA cm^{-2})	Reference
Vertical graphene@SiO	1.3 m Ah cm^{-2} (100)	~92.8%	0.48 mA cm^{-2}	[25]
Nonfilling carbon-coated porous Si microparticle	2.84 m Ah cm^{-2} (100)	-	0.25 mA cm^{-2}	[1]
Polyrotaxane-PAA binder@Si microparticle	2.67 m Ah cm^{-2} (150)	91%	0.64 mA cm^{-2}	[26]
Si@CNT coaxial fiber	1.25 m Ah cm^{-2} (50)	-	0.26 mA cm^{-2}	[27]
SiO$_2$@TiO$_2$ core-shell	1.07 m Ah cm^{-2} (200)	<50%	0.26 mA cm^{-2}	[28]

References

1.	Z. Lu, N. Liu, H.-W. Lee, J. Zhao, W. Li, Y. Li and Y. Cui, *ACS Nano*, 2015, **9**, 2540-2547.
2.	J. Zhu, T. Wang, F. Fan, L. Mei and B. Lu, *ACS Nano*, 2016, **10**, 8243-8251.
3.	F. Maroni, G. Carbonari, F. Croce, R. Tossici and F. Nobili, *ChemSusChem*, 2017, **10**, 4771-4777.
4.	Y. Xing, T. Shen, T. Guo, X. Wang, X. Xia, C. Gu and J. Tu, *J. Power Sources*, 2018, **384**, 207-213.
5.	H. Wu, G. Yu, L. Pan, N. Liu, M. T. McDowell, Z. Bao and Y. Cui, *Nat. Commun.*, 2013, **4**, 1943.
6.	A. Casimir, H. Zhang, O. Ogoke, J. C. Amine, J. Lu and G. Wu, *Nano Energy*, 2016, **27**, 359-376.
7.	Y. Jin, B. Zhu, Z. Lu, N. Liu and J. Zhu, *Adv. Energy Mater.*, 2017, **7**, 1700715.
8.	X.-y. Zhou, J.-j. Tang, J. Yang, J. Xie and L.-l. Ma, *Electrochim. Acta*, 2013, **87**, 663-668.
9.	X. Xiao, W. Zhou, Y. Kim, M. Gu, C. Wang, G. Liu, Z. Liu and H. Gao, *Adv. Funct. Mater.*, 2015, **25**, 1426-1433.
10.	Y. Chen, M. Nie, B. L. Lucht, A. Saha, P. R. Guduru and A. Bose, *ACS Appl. Mater. Interfaces*, 2014, **6**, 4678-4683.
11.	S. Choi, D. S. Jung and J. W. Choi, *Nano Lett.*, 2014, **14**, 7120-7125.
12.	B.-S. Lee, H.-S. Yang, H. Jung, S.-Y. Jeon, C. Jung, S.-W. Kim, J. Bae, C.-L. Choong, J. Im and U.-I. Chung, *Nanoscale*, 2014, **6**, 5989-5998.
13.	L. Shi, W. Wang, A. Wang, K. Yuan, Z. Jin and Y. Yang, *J. Mater. Chem. A*, 2015, **3**, 18190-18197.
14.	H. Park, S. Choi, S. Lee, G. Hwang, N.-S. Choi and S. Park, *J. Mater. Chem. A*, 2015, **3**, 1325-1332.
15.	N. T. Hieu, J. Suk, D. W. Kim, J. S. Park and Y. Kang, *J. Mater. Chem. A*, 2014, **2**, 15094-15101.
16.	W. Li, Z. Li, W. Kang, Y. Tang, Z. Zhang, X. Yang, H. Xue and C.-S. Lee, *J. Mater. Chem. A*, 2014, **2**, 12289-12295.
17.	J. Wu, X. Qin, C. Miao, Y.-B. He, G. Liang, D. Zhou, M. Liu, C. Han, B. Li and F. Kang, *Carbon*, 2016, **98**, 582-591.
18.	T. Jaumann, M. Herklotz, M. Klose, K. Pinkert, S. Oswald, J. r. Eckert and L. Giebeler, *Chem. Mater.*, 2014, **27**, 37-43.
19.	J. Wang, X. Meng, X. Fan, W. Zhang, H. Zhang and C. Wang, *ACS Nano*, 2015, **9**, 6576-6586.
20.	B. Li, F. Yao, J. J. Bae, J. Chang, M. R. Zamfir, D. T. Le, D. T. Pham, H. Yue and Y. H. Lee, *Sci. Rep.*, 2015, **5**, 7659.
21.	N. Liu, H. Wu, M. T. McDowell, Y. Yao, C. Wang and Y. Cui, *Nano Lett.*, 2012, **12**, 3315-3321.
22.	B. Wang, X. Li, X. Zhang, B. Luo, Y. Zhang and L. Zhi, *Adv. Mater.*, 2013, **25**, 3560-3565.
23.	B. Lu, B. Ma, X. Deng, W. Li, Z. Wu, H. Shu and X. Wang, *ACS Appl. Mater. Interfaces*, 2017, **9**, 32829-32839.
24.	S. Fang, Z. Tong, P. Nie, G. Liu and X. Zhang, *ACS Appl. Mater. Interfaces*, 2017, **9**, 18766-18773.
25.	L. Shi, C. Pang, S. Chen, M. Wang, K. Wang, Z. Tan, P. Gao, J. Ren, Y. Huang and H. Peng, *Nano Lett.*, 2017, **17**, 3681-3687.
26.	S. Choi, T.-w. Kwon, A. Coskun and J. W. Choi, *Science*, 2017, **357**, 279-283.
27.	Q. Xiao, Y. Fan, X. Wang, R. A. Susantyoko and Q. Zhang, *Energy Environ. Sci.*, 2014, **7**, 655-661.
28.	J. Yang, Y. Wang, W. Li, L. Wang, Y. Fan, W. Jiang, W. Luo, Y. Wang, B. Kong and C. Selomulya, *Adv. Mater.*, 2017, **29**, 1700523.